A Three-Degrees-of-Freedom Micromotion In-Parallel Actuated Manipulator

Kok-Meng Lee, *Member, IEEE,* and Shankar Arjunan

Abstract—**The advancement of microminiaturization and technologies has motivated the search for a technique that will permit precision manipulation on the scale of micrometers. This paper presents the development of a three-degrees-of-freedom (DOF) micromotion in-parallel actuated manipulator. The micromotion manipulator, which has one translation and two orientation freedoms, is actuated by piezoelectric effect. In particular, the paper presents a closed-form solution and an experimental verification of the forward kinematics. In addition, the dynamic model of the piezoelectric actuated link was determined experimentally providing a rational basis for the design and prismatic joint force control of the high-speed micromotion manipulator. A special configuration that approaches an optimal design, in terms of working range, rigidity, and bandwidth, has also been highlighted.**

I. Introduction

THIS paper presents the development of a three-degrees-of-freedom (3-DOF) micromotion in-parallel actuated manipulator using piezoelectric elements. Because the multilayer piezoelectric actuator has the advantages of fast response, high resolution, and high force generation per unit volume, the micromotion manipulator has potential applications where high-speed precision manipulation on the scale of micrometers is required. Typical applications include the assembly of optical components and delicate mechanical devices.

The revolutionary impact that microminiaturization has had on electronics seems to indicate the benefit of extending the concept to other fields [1]–[4] such as integrated optics and microdevices [5]–[10]. However, despite the development of unusual electromechanical actuators for robotic applications, industrial robots have been recognized as having limited static accuracy for microminiaturization applications due to measurement errors, poor rigidity, and nonlinearities of the actuators. In the control of a manipulator, the end-point position and orientation are generally fed back by measuring the joint angles followed by a forward kinetic computation. There are two difficulties encountered in practical implementation. First, the forward kinematics of the robotic manipulator requires time-consuming numerical computation. Second, the feedback information is indirect, and hence the dynamic effects of the manipulator on each individual joint must be normally accounted for. To alleviate this problem, the concept of a coarse–fine motion control strategy to enhance robot accuracy was suggested by Sharon and Hardt [11] and Hollis [12]. A planar XY robotic fine positioning device was developed for end-point sensing [13], and successful application experiments on circuit inspection were reported in [14]. Hollis *et al.* [15] recently developed an interesting design for a six-degrees-of-freedom fine-motion "magic wrist" on the basis of magnetically levitated variable compliance.

Piezoelectric actuators present an alternate solution to micromotion control. Bruning [16] demonstrated that an incremental displacement of 0.05 to 2 μm over a range of centimeters could be achieved using the piezoelectric effect in the design of a linear stepping device. Scire and Teague [17] developed a linear micropositioning stage using a piezoelectric driving element and flexure pivots to achieve a resolution of 0.001 μm over a range of 50 μm. The advantages of flexure pivots, which are characterized by having no backlash, friction, and bearing noise over bearings and sliding components, were demonstrated. Umetani and Suzuki [18], [19] presented the principle of a piezoelectric micromanipulator. The design of linear and multi-DOF motion actuators based on the piezoelectric effect has also been reported in [20]–[22]. The advantages of fast response, high resolution, and high force generation per unit volume are obtainable from the multilayer piezoelectric actuator and have motivated the development of a series-parallel micromotion mechanism [23] as a wrist torque sensor and have been used to enhance the resolution of an innovative spherical motor. The design of a piezoelectric actuated manipulator with two orientation and one translation freedoms was conceptualized by Lee and Arjunan [24]. Recently, Hunter *et al.* [25], [26] reported the progress of a microrobot design using the dual actuator approach for manipulation and dynamic testing of a single living cell, which is essentially an in-parallel actuated micropositioning device in a spherical coordinate. The analysis of a polymeric piezoelectric bimorph as a distributed sensor and actuator was performed by Tzou *et al.* [27], [28] for vibration control of a light-weight arm. A general discussion of actuators for microrobots has been presented by Trimmer and Jebens [29].

The design and dynamic modeling of a 3-DOF micromotion in-parallel manipulator actuated by piezoelectric elements is considered in this paper. The kinematic, dynamic, and static characteristics of the mechanism as a coarse motion manipulator were discussed by Lee and Shah [30], [31] and by Lee and Johnson [32]. In particular, this paper focuses on

Manuscript received September 26, 1988; revised November 27, 1990. This work was supported under a Graduate Research Assistantship from the Georgia Tech Computer Integrated Manufacturing Systems Program and was presented at the IEEE International Conference on Robotics and Automation, May 14–19, 1989, Scottsdale, AZ.

K.-M. Lee is with the George W. Woodruff School of Mechanical Engineering, Georgia Institute of Technology, Atlanta, GA 30332-0405.

S. Arjunan is with the Cummins Engine Company, Columbus, IN 47201.

IEEE Log Number 9101346.

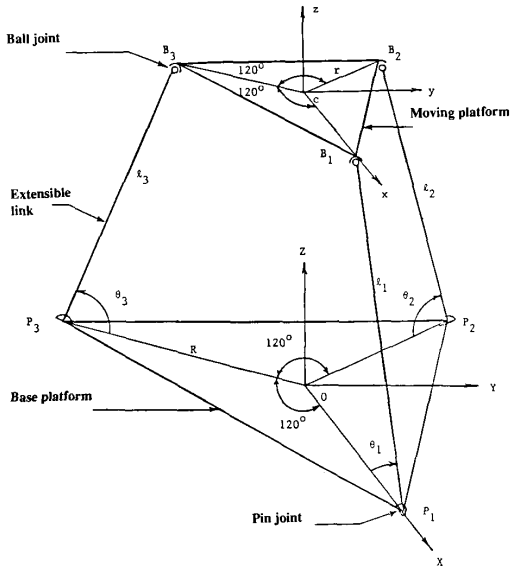

Fig. 1. Schematics of a three-DOF in-parallel actuated manipulator.

the closed-form solution and experimental verification of forward kinematics for micromotion control. To provide a rational basis for the control of high-speed micromotion manipulation using the piezoelectric actuation, the dynamic model of a micromotion manipulator was determined experimentally.

II. Kinematics

A schematic of the 3-DOF in-parallel actuated manipulator is shown in Fig. 1. The manipulator consists of a base platform, three extensible links, and a moving platform that houses the driving mechanism of the gripper. The moving platform is connected to the links by means of ball joints that are equally spaced at 120° and at a radius r from the center of the moving platform. The other ends of the links are connected to the base platform through equally spaced pin joints at a radius R from the center of the base platform. By varying the link lengths, the moving platform can be manipulated with respect to the base platform. It has been shown by Lee and Shah [30] that the manipulator has one translation and two orientation freedoms. A closed-form solution of the inverse kinematics has been derived in [30]. It is also useful to derive a linearized closed-form forward kinematic relationship, which determines the translation in the z direction and the rotations about the X and Y axes of the base coordinate for a given set of link lengths.

The coordinate system is shown in Fig. 1. A base coordinate frame XYZ, with unit vectors i, j, and k, respectively, is fixed at the center of the base platform with the Z axis pointing vertically upward and the X axis pointing toward pin joint P_1. Similarly, a coordinate frame xyz is assigned to the center of the movable platform with the z axis normal to the platform and the x axis pointing toward ball joint B_1. The forward kinematics is derived using the following procedure. The angle subtended between the ith link and the base platform θ_i as shown in Fig. 1 is determined as a function of the given link lengths. Next, the coordinates of the ith ball joint are determined in terms of the link lengths and the subtended angles. Finally, the position and orientation of the moving platform are computed from the known coordinates of the ball joints.

As the distance between the adjacent ball joints is $r\sqrt{3}$, the implicit relationship between the link lengths and the subtended angles is [30]

$$L_i^2 + L_j^2 + 3 - 3\rho^2 + L_iL_j\cos\theta_i\cos\theta_j - 2L_iL_j\sin\theta_i\sin\theta_j - 3L_i\cos\theta_i - 3L_j\cos\theta_j = 0 \quad (1)$$

where $i = 1, 2, 3$; $j = 2, 3, 1$; $L_i = l_i/R$; and $\rho = r/R$. Equation (1) is of the following form:

$$f_i(\theta_i, \theta_j, L_i, L_j) = 0, \qquad i = 1, 2, 3 \text{ and } j = 2, 3, 1.$$

Since the motion is in the order of micrometers, a closed-form solution can be derived by linearization about an operating point, $\theta_i = \theta_0$ and $L_i = L_0$ where $i = 1, 2, 3$. For a specified L_0 the corresponding operating angle θ_0 is determined from the geometry:

$$\cos\theta_0 = R(1 - \rho)/L_0.$$

By expanding $f_i(\theta_i, \theta_j, L_i, L_j)$ in a Taylor series and noting that

$$\left.\frac{\partial f_i}{\partial \theta_i}\right|_{\theta_0, L_0} = \left.\frac{\partial f_i}{\partial \theta_j}\right|_{\theta_0, L_0} = c_1$$

and

$$\left.\frac{\partial f_i}{\partial L_i}\right|_{\theta_0, L_0} = \left.\frac{\partial f_i}{\partial L_j}\right|_{\theta_0, L_0} = c_2$$

where

$$c_1 = 3L_0\sin\theta_0[1 - L_0\cos\theta_0]$$
$$c_2 = -3\cos\theta_0[1 - L_0\cos\theta_0]$$

the linearized equation about an operating point (θ_0, L_0) is

$$\Delta\theta_i + \Delta\theta_j = -\frac{c_2}{c_1}(\Delta L_i + \Delta L_j) \quad (2)$$

where $\Delta\theta = \theta - \theta_0$, $\Delta L = L - L_0$, and the subscripts denote the respective links $i = 1, 2, 3$ and $j = 2, 3, 1$. For a given set of link lengths, $\Delta\theta_i$ can be derived by solving the three constraint equations simultaneously. The result is

$$\Delta\theta_i = \frac{\Delta L_i}{L_0\tan\theta_0} \quad (3)$$

where $\tan\theta_0 \neq 0$. The three linearized equations, i.e., (3) with $i = 1, 2, 3$, are decoupled. Also, in the linearized range, the change of the subtended angle of ith link with the base platform $\Delta\theta_i$ is linearly proportional to the change of the respective link length ΔL_i. It is noted that θ_0 corresponds to a singular point, and when $\theta_0 = \pi/2$, the change in link length is accompanied with no change in the subtended angle.

A. Cartesian Position of Moving Platform

Since the ball joints are placed at the vertices of an equilateral triangle, the Cartesian position or the origin of the xyz frame is essentially the centroid of the triangle. The Cartesian coordinates of the ith ball joint are

$$X_{Bi} = (1 - L_i \cos\theta_i) \cos\left[\tfrac{2}{3}(i-1)\pi\right] \quad (4a)$$

$$Y_{Bi} = (1 - L_i \cos\theta_i) \sin\left[\tfrac{2}{3}(i-1)\pi\right] \quad (4b)$$

$$Z_{Bi} = L_i \sin\theta_i. \quad (4c)$$

and the coordinates of the origin of the moving platform are

$$X_c = \tfrac{1}{3}\sum_{i=1}^{3} - L_i \cos\theta_i \cos\left[\tfrac{2}{3}(i-1)\pi\right] \quad (5a)$$

$$Y_c = \tfrac{1}{3}\sum_{i=1}^{3} - L_i \cos\theta_i \sin\left[\tfrac{2}{3}(i-1)\pi\right] \quad (5b)$$

$$Z_c = \tfrac{1}{3}\sum_{i=1}^{3} L_i \sin\theta_i. \quad (5c)$$

B. Orientation of Moving Platform

With the coordinates of the ball joints described in terms of the link lengths and the subtended angles, the unit vectors of the body axes xyz with respect to the base coordinate XYZ are given in (6)–(8)

$$\vec{u}_x = \frac{\vec{OB}_1 - \vec{OC}}{r} \quad (6)$$

$$\vec{u}_y = \frac{\vec{OB}_2 - \vec{OB}_3}{\sqrt{3}\, r} \quad (7)$$

$$\vec{u}_z = \vec{u}_x \times \vec{u}_y \quad (8)$$

where OB_i is the line vector originating from the point O to the center of the ith ball joint, and OC is the line vector originating from the point O to the center of moving platform C.

The orientation will be described in terms of rotation about the X and Y axes of the base coordinate. The rotations about the X and Y axes are designated as α and β, respectively. The transformation matrix, which describes the coordinate transformation of the xyz body axes with respect to the base coordinate XYZ, is given by

$$[\mathrm{ROT}] = \begin{vmatrix} \cos\beta & \sin\beta\sin\alpha & \sin\beta\cos\alpha \\ 0 & \cos\alpha & -\sin\alpha \\ -\sin\beta & \cos\beta\sin\alpha & \cos\beta\cos\alpha \end{vmatrix}. \quad (9)$$

Hence, the unit vectors of the body axes have been derived in (6)–(8), the components of which are the elements of the matrix [ROT]:

$$[\mathrm{ROT}] = \begin{vmatrix} u_{xi} & u_{yi} & u_{zi} \\ u_{xj} & u_{yj} & u_{zj} \\ u_{xk} & u_{yk} & u_{zk} \end{vmatrix}. \quad (10)$$

From (9) and (10), the angles α and β can be obtained by the following relations:

$$\alpha = \tan^{-1}(u_{yk}/u_{zk}) \quad (11)$$

$$\beta = \tan^{-1}(u_{zi}/u_{zk}) \quad (12)$$

and the angle of rotation about the z axis is

$$\gamma = \cos^{-1} u_{xi}. \quad (13)$$

The solution of the forward kinematics can be computed as follows: The change of subtended angle $\Delta\theta_i$ is determined using (3). The Cartesian position of the ball joints and the center of the moving platform can then be computed using (4) and (5). The angles of rotation about the X and Y axes, α and β, can then be computed from (11) and (12) where the unit vectors of the body axes are given in (6)–(8).

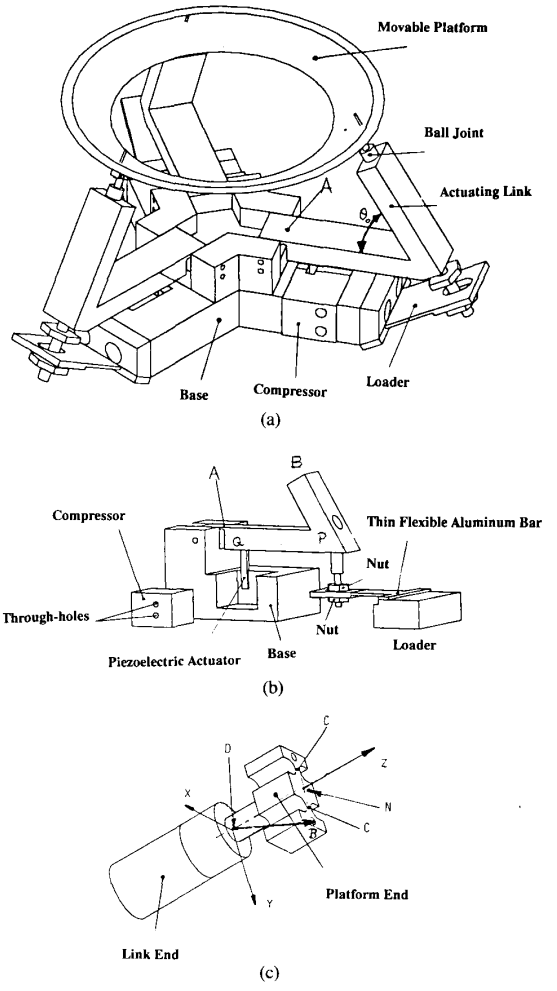

Fig. 2. (a) Schematics of a prototype micro-motion manipulator. (b) Typical prototype link design. (c) Typical prototype ball joint design.

III. Prototype Micromotion Manipulator

The design of a prototype manipulator is shown in Fig. 2. The prototype links that provide motion in the order of micrometers were actuated by the piezoelectric actuator as

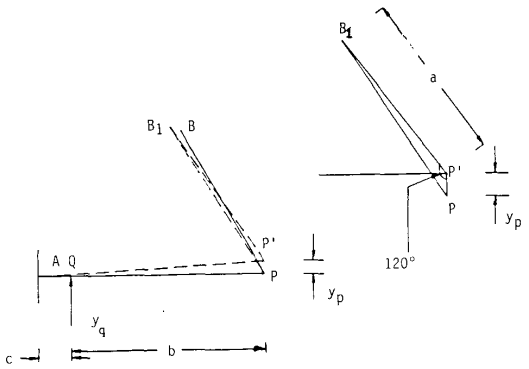

Fig. 3. Virtual pin joint.

shown in Fig. 2(a). All components were assembled and tightly fixed by means of solid pins in order to eliminate any possible relative motion.

The link design consists of a cantilever structure that flexes at pivot points A when the actuation is provided at Q. The cantilever structure is to enable amplification of motion generated by the piezoelectric actuator located at Q. Unlike the flexure pivot design in [17], the flexure pivot at A was designed to have a notch on only one side of the beam to allow a strain gage attachment. This design enables the link motion to be inferred from the strain gage measurement. The piezoelectric element was clamped between the base and the compressor. The compressor is a rigid element designed to align and to secure the actuator in place using pressure exerted by a pair of screws fastened into the through-holes. The loader behaves as a rotational spring to ensure a positive contact between the actuator and the link and thus eliminates the backlash. The stiffness of the loader was designed to be much less than that of the pivot point at A so that the dynamic effect of the loader can be neglected.

The equivalent change in link length ΔL and $\Delta\theta$ of the prototype link design can be derived by regarding point P as a virtual pin joint. The argument is substantiated as shown in Fig. 3 where point P is the initial position and point P' is the corresponding position after the cantilever has been actuated by the piezoelectric actuator at Q. Similarly, point B has been moved to B_1 after the actuation. Hence, the angle that is subtended between lines PB and PB_1 is the angle of rotation about the virtual joint P. Length PB_1 can be derived by applying the aw of cosines to the triangle $PP'B_1$ shown in Fig. 3:

$$(PB_1)^2 = (PB)^2 + (PP')^2 - 2(PB) \cdot (PP') \cos\left(\theta_0 + \frac{\pi}{2}\right)$$

where θ_0 is the angle between the lines AP and PB.

From geometry, the deflection at P, PP', is approximated by $(b/c)y_q$ where y_q is displacement at Q

$$\left[\frac{PB_1}{PB}\right]^2 = 1 + 2\frac{by_q}{ca}\sin\theta_0 + \left(\frac{by_q}{ca}\right)^2$$

where a, b, and c are the lengths PB, QP, and AQ, respectively. Using the technique of series expansion and neglecting the higher order terms of $(b/ac)y_q$, the change in link length is given as

$$\Delta L = PB_1 - PB = \frac{b}{c}y_q \sin\theta_0. \tag{14}$$

The underlying assumption of (14) is that the geometry $(b/ac)y_q$ must be much smaller than unity. Hence, the prototype link design has a virtual pin joint at P and has an effective change in link length given in (14).

The function of the ball joint, as shown in Fig. 2(b), is to provide three rotational degrees of freedom. The thin cylindrical cross section at A allows bending about the x and y axes. The thin section at C enables rotation about the Z axis as seen in the figure. The neutral axes are BN for bending about the x and y axes and ND for the bending about z axis. The structure of the ball joint is such that the length of the vector BD that connects point B and pin location D remains a constant. Hence, the structure has a virtual ball joint with its center at B and an effective radius equal to BD. The ball joint was rigidly attached to the movable platform at D, which was constructed in the shape of the frustum of a cone as shown in Fig. 2.

TABLE I
PARAMETERS OF PIEZOELECTRIC ACTUATED LINK

Piezoelectric:	TOKIN NLA 2 × 3 × 18
Maximum Travel:	10 μm
Force Generation:	350 kg/cm^2
Link Geometry:	a = 50 mm
	b = 5 mm
	c = 18 mm
	θ_0 = 60°
Aluminum Cross Section:	10 mm × 13.5 mm
Pin Cross Section:	0.508 mm × 13.5 mm

The parameters of the link and the specifications of the piezoelectric actuator are listed in Table I. The piezoelectric element used in the experiment was TOKIN 2 × 3 × 18 [33], where the numerical values are the physical dimensions in millimeters. The piezoelectric element has a linear range of 0–15 μm corresponding to 0–150-V input. The multilayer piezoelectric actuator has a relatively dielectric constant of 13.5 μm per 100 V as compared to that of 0.22 and 15 μm/kV reported in [17] and [34], respectively. The multilayer piezoelectric actuator has a higher force generation than that reported in [22], [25], and [27].

A. Experimental Results of Kinematics

Since the motion is very small, it is almost imperceptible to the human eye. To verify the kinematics of the micromotion manipulator and to demonstrate the concept feasibility, a mirror was attached to the movable platform and a laser beam was directed toward the mirror. The reflected beam is seen on the wall at a distance of about 9 m (30 ft). When the platform is oriented, the deflection of the laser beam on the wall is measured. From the correlation between the beam deflection and the angle of rotation of the moving platform, the kinematics was determined and verified.

1) Correlation Between Experiments and Analysis: When

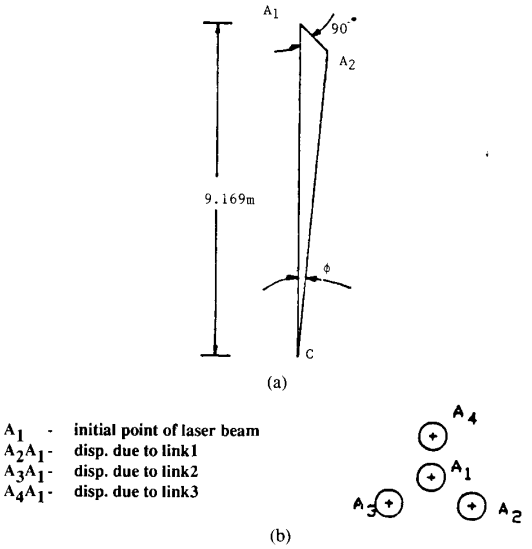

Fig. 4. (a) Determination of rotation angle. (b) Beam movement.

a step input is applied to one of the links, the moving platform and hence the mirror rotates about both the x and y axes. As the measured deflection indicates a net rotation of the moving platform, the following steps were taken to correlate the experimental data to the forward kinematics. When the beam is directed to the center of the moving platform, denoted as C, it reflects from position A_1 to A_2 as shown in Fig. 4(a). Consider the triangle CA_1A_2, where ϕ is the angle of rotation reflected by the laser beam. From the geometry, the angle ϕ can be determined as $\tan^{-1}(A_1A_2/CA_1)$ where A_1A_2 is beam deflection on the wall to be measured experimentally and CA_1 is predetermined distance of 9 m. It is known from the law of physics that when a mirror is turned through an angle ψ, the reflected beam is rotated through 2ψ. In other words, since the reflected beam travels through ϕ, the plate should have rotated through $\phi/2$. Hence, by measuring the distance of the center of the beam before and after moving each link, the angle of rotation can be inferred.

Since link 1 is located in the $Y = 0$ plane, the platform will rotate only about the Y axis if only link 1 is actuated. Hence, there is a direct correlation between the angle of rotation about the y axis, and the angle of rotation of the reflected beam is determined experimentally. However, if only link 2 is actuated, the plate will rotate about the line joining ball joints B_1 and B_3. By constructing the vectors directed from the midpoint between B_1 and B_2, to point C, before and after the motion of link 2, it can be deduced that the angle between these two vectors is essentially the angle of rotation of the moving platform. Similarly, if only link 3 is actuated, the plate will rotate about the line joining ball joints B_1 and B_2.

2) Experimental Verification: The experiments were conducted by actuating one of the links at a time, and the steady-state positions of the beam on the wall before and after the actuation were tracked. The beam's movement is shown in Fig. 4(b). For an input of 100 V to one of the links, the image of the beam moved a distance of 6.75 mm (0.27 in), 8 mm (0.32 in), and 6.25 mm (0.25 in), corresponding to the actuation of links 1, 2, and 3, respectively. The points were half-way in each direction for an input of 50 V and thus verified that the motion is linear within the range tested. Although the kinematics of the micromotion manipulator is linear with respect to the link displacement, the hysteresis effect of the piezoelectric actuator may introduce a nonlinearity to the overall system control. As the beam deflection was rather insensitive to z displacement, no attempt was made to measure the z motion directly.

TABLE II
EXPERIMENTAL DATA

Link Actuation	Angle of Rotation Experimental	Angle of Rotation Analytical
Link 1	$-0.02142°$	$-0.0227°$ ($\alpha = 0$, $\beta = -0.0227°$)
Link 2	$0.02539°$	$0.02806°$ ($\alpha = 0.0247°$, $\beta = 0.0143°$)
Link 3	0.01983	$0.02099°$ ($\alpha = -0.0187°$, $\beta = 0.01496°$)

To determine the end-point position for the link actuation, the linearized forward kinematics was employed. The changes in link length were determined from the strain gage outputs, and the rotations about the X and Y axes were then determined from (3)–(7). To compare the analytical and experimental data, the angles of platform rotation were calculated. The results are summarized in Table II. The analytical results are in agreement with the experimental data. The steady-state end-point position/orientation of the micromotion manipulator can be determined rather accurately from the simple closed-form forward kinematics.

B. Dynamic Model of Actuating Link

In the prismatic joint force control of the micromotion manipulator, it is expected that the link dynamics have significant influence on the end-point accuracy of the moving platform. The dynamic effects of the moving platform and the payload on the individual link control can be considered as reaction forces acting at the ball joints. It is of interest to determine the dynamic model of the link actuated by the piezoelectric element. The dynamic model was obtained experimentally using the standard frequency response technique with a HP3562A dynamic analyzer.

The experimental setup is shown in Fig. 5. The output signal of the HP analyzer was fed to a Kepco power amplifier having a gain of 10, which in turn drove the piezoelectric actuator. The actuation would displace the link, which is sensed by means of a strain gage that is located at the flexure point A on the link. The strain gage is part of a wheatstone bridge, the output from the bridge is fed into a Analog Devices 3B18 signal conditioning amplifier for filtering and signal amplification. The conversion factor of combined strain gage calibration and 3B18 amplification was 1.3 V/mm. The bandwidths of the power amplifier and the signal conditioning amplifier were 3 and 20 kHz, respectively.

The frequency response data were collected with the input

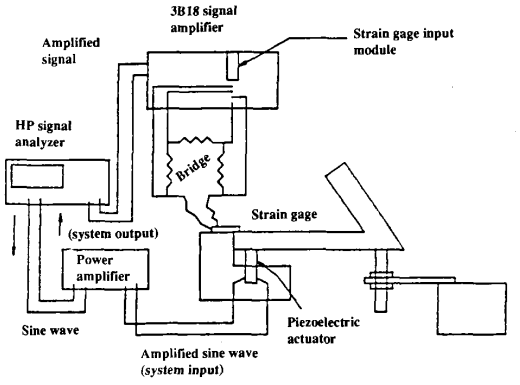

Fig. 5. Experimental setup for dynamic model determination.

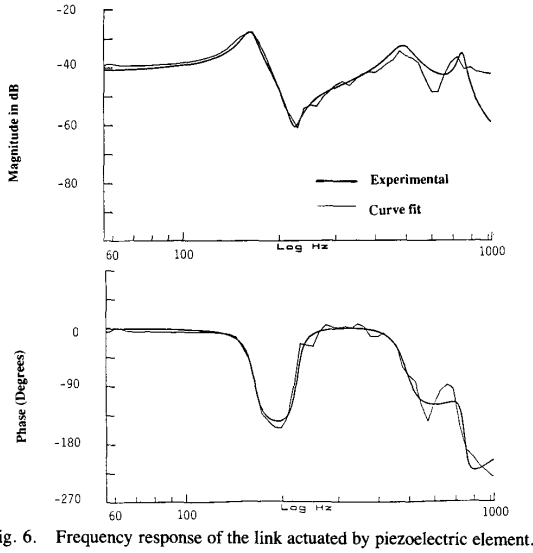

Fig. 6. Frequency response of the link actuated by piezoelectric element.

voltage to the piezoelectric element limited between 25–75 V. The Bode plots obtained experimentally are displayed in Fig. 6. With the link actuation approximated as a simple mass-spring system where the stiffness of the flexural joint and the preload spring were 250 and 4.2 kN/m, respectively, the natural frequency was found analytically to be 185 Hz. With the aid of the curve-fitting function in an HP Analyzer, three pairs of complex zeros and poles were identified as follows:

Poles are:	Zeros are:
$-8.7739 \pm j163.899$	$-8.547 \pm j223.336$
$-41.3206 \pm j489.184$	$-161.24 \pm j751.483$
$-18.7336 \pm j749.497.$	$-79.812 \pm j1294.9.$

The curve fits well and approximates the experimental data up to the frequency of 1000 Hz as shown in the comparison in Fig. 6. Hence, the link dynamics is characterized by the following transfer function:

$$\frac{Y_q(s)}{V(s)} = K \prod_{i=1}^{3} \frac{s^2 + a_{1i}s + a_{0i}}{s^2 + b_{1i} + b_{0i}} \tag{15}$$

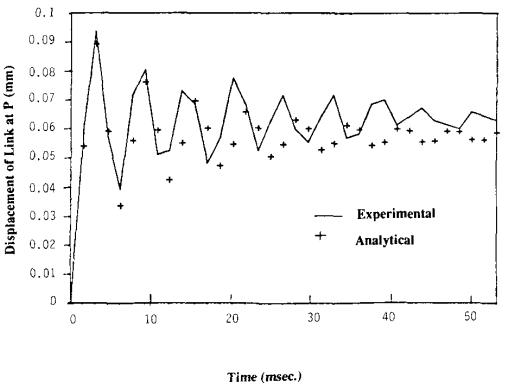

Fig. 7. Open-loop step response.

where

$$K = 5.93E - 5$$
$$a_{01} = 1.97E + 6 \quad a_{02} = 2.24E + 7 \quad a_{03} = 6.63E + 7$$
$$a_{11} = 110 \quad a_{12} = 2009 \quad a_{13} = 1005$$
$$b_{01} = 1.06E + 6 \quad b_{02} = 9.51E + 6 \quad b_{03} = 2.23E + 7$$
$$b_{11} = 110 \quad b_{12} = 519 \quad b_{13} = 235$$

and where s is a Laplacian operator, $V(s)$ is the input voltage to the piezoelectric element, and $Y_q(s)$ is the displacement measured at Q in millimeters. It is of interest to verify the experimentally determined transfer function of the link in the time domain. A step input of 75 V was applied to the actuator, and the strain gage output data were sampled at 20 kHz digitally using an IBM PC/XT with Metrabyte Dash-16 data acquisition hardware. It can be seen from Fig. 7 that the experimental data and the analytical data are in agreement and exhibited all the dynamics involved. The two graphs do not match perfectly, but they exhibit how the higher order frequencies are dominant in the response. The higher order frequency components are due primarily to the piezoelectric elements, which have also been observed and discussed qualitatively as vibration in [17].

IV. Special Configuration

A special configuration corresponding to $\theta_0 = 90°$ is worth noting. For $\theta_0 = 90°$, which implies $R = r$, (3) indicates that a change in link length ΔL_i is not accompanied by a change in subtended angle $\Delta\theta i$, as shown in (3). It follows, from the forward kinematics equations, that the end-point position and orientation are

$$X_c = Y_c = \gamma = 0$$
$$\Delta Z_c = \tfrac{1}{3}(\Delta L_1 + \Delta L_2 + \Delta L_3) \tag{16a}$$
$$\alpha = \frac{1}{\sqrt{3}}(\Delta L_2 - \Delta L_3) \tag{16b}$$
$$\beta = \Delta L_1 - \Delta Z_c. \tag{16c}$$

The corresponding linearized inverse kinematics are

$$\Delta L_1 = \Delta Z_c + \beta \tag{17a}$$

$$\Delta L_2 = \Delta Z_c - \tfrac{1}{2}\beta + \frac{\sqrt{3}}{2}\alpha \tag{17b}$$

$$\Delta L_3 = \Delta Z_c - \tfrac{1}{2}\beta - \frac{\sqrt{3}}{2}\alpha. \tag{17c}$$

The linearized forward and inverse kinematics are given in (16) and (17), respectively. This special case, where $\theta_0 = \pi/2$ radius, indicates that the micromotion control of α, β, and Z_c can be achieved without any accompanying change in X_c, Y_c, and γ. The work envelop is such that the maximum values of α and β decrease from a maximum at $\Delta Z_c = 0$ to zero at $\Delta Z_c = \pm Y_{\max}$. It is interesting to note that the kinematics is independent of l_0.

From the principle of virtual work, it can be shown that the static force relationship between the Cartesian moment-force vector acting at the moving platform $[T_x, T_y, F_z]$ and the joint force vector $[F_1, F_2, F_3]$ is

$$\begin{bmatrix} F_1 \\ F_2 \\ F_3 \end{bmatrix} = \begin{bmatrix} 0 & \frac{2}{3} & \frac{1}{3} \\ \frac{1}{\sqrt{3}} & -\frac{1}{3} & \frac{1}{3} \\ -\frac{1}{\sqrt{3}} & -\frac{1}{3} & \frac{1}{3} \end{bmatrix} \begin{bmatrix} \frac{T_x}{R} \\ \frac{T_y}{R} \\ F_z \end{bmatrix} \tag{18}$$

where F_i, $i = 1, 2, 3$, is the actuating force perpendicular to the moving platform through the ball joint; T_x and T_y are the torques acting about the X and Y axes and the force acting in the Z direction, respectively. F_i can be approximated as $(c/b)\,F_p$ where F_p is the force actuated by the piezoelectric elements. Hence, the measurements of F_i allow the Cartesian moment force vector to be determined by (18).

In this particular configuration, the micromotion manipulator provides the actuating torques about X and Y axes and an actuating force along the Z direction. Any external moments about the Z axis, T_z, or external forces along the X and Y axes, F_x and F_y, must be supported by the joints in the form of reaction forces. The external forces F_x and F_y would result in bending moments equal to $F_x l_0$ and $F_y l_0$ on the links. However, as the range of motion in independent of l_0 in the $\theta_0 = \pi/2$ configuration, the bending movements on the link can be reduced to a minimum or to zero, using a design with minimum l_0 or $l_0 = 0$, respectively. In addition, the possibility of reducing l_0 to a minimum or to zero value has a potential to further increase the bandwidth of the manipulator.

The motion of the individual link that is subjected to reaction forces at the ball joints can be controlled using strain gage feedback. Although end-point sensing can be achieved using a laser scanning technique, the special configuration with small or zero l_0, which would result in a close proximity between the moving platform and the base platform, offers an alternative means of end-point sensing using miniature forceps between the moving platform and the base platform. An example of miniature forceps designed on the basis of microbending in fiber optics can be found in [35], which is currently being investigated for the closed-loop end-point control of a micromotion manipulator.

V. Conclusion

The design concept of a 3-DOF micromotion in-parallel actuated manipulator using piezoelectric elements for actuation has been examined and developed. The development has indicated that high-speed micromotion manipulation can be achieved using piezoelectric actuation.

In particular, the closed-form kinematics for micromotion manipulation has been derived and experimentally verified. A special configuration corresponding to $\theta = \pi/2$ would result in the micromotion control of α, β, and Z_c accompanied with no change in the subtended angles, and, thus, no changes in X_c, Y_c, and γ. As the kinematics is independent of l_0, the special configuration approaches an optimal design in terms of working range, rigidity, and bandwidth. The static force relationship between the joint space and the task space is given, which is useful for 3-DOF force/torque sensing.

The dynamic model of the piezoelectric actuated link has been determined experimentally, which provides a rational basis for the design and for prismatic joint force control of the high-speed micromotion manipulator. The studies have indicated that significant high-order frequency components due to the piezoelectric actuation are presented in the link dynamics.

References

[1] A. J. Blodgett, Jr., "Microelectronic packaging," *Sci. Amer.*, pp. 86-96, July 1983.

[2] G. M. Robinson, "How advanced motion control enhances cancer treatment," *Design News*, pp. 72-76, Sept. 21, 1987.

[3] G. Haugen, "Micro miniaturization is finding application beyond electronics," *Res. Develop.*, pp. 66-69, Mar. 1987.

[4] N. Taniguchi, "Current status in, and future trends of, ultraprecision machining and ultrafine materials processing," *CIRP Ann.*, vol. 32, no. 2, pp. 573-582, 1983.

[5] W. S. N. Trimmer and K. J. Gabriel, "Design considerations for a practical electrostatic micro-motor," *Sensors Actuators*, vol. 11, pp. 189-206, 1987.

[6] M. M. Mehregany, K. J. Gabriel, and W. S. N. Trimmer, "Micro gears and turbines etched from silicon," *Sensors Actuators*, vol. 12, pp. 341-348, 1987.

[7] H. Fujita, "Studies of micro actuators in Japan," in *Proc. Int. Conf. Robotics Automat.* (Scottsdale, AZ, May 14-19, 1989), pp. 1559-1565.

[8] S. C. Jacobsen, R. H. Price, J. E. Wood, T. H. Rytting, and M. Rafaelof, "The wobble motor: Design, fabrication and testing of an eccentric-motion electrostatic microactuator," in *Proc. IEEE Int. Conf. Robotics Automat.* (Scottsdale, AZ, May 14-19, 1989), pp. 1535-1546.

[9] J. H. Lang, M. F. Scklecht, and R. T. Howe, "Electric micromotors: Electromechanical characteristics," in *Proc. IEEE Micro-Robots Teleoperators Workshop* (Hyannis, MA, Nov. 9-11, 1987).

[10] P. Lebet, "Assembly with robots in micro-engineering," in *Proc. Int. Conf. Assembly Automation*, 1982, pp. 29-40.

[11] A. Sharon and D. Hardt, "Enhancement of robot accuracy using endpoint feedback and a macro-micro manipulator system," in *Proc. Amer. Control Conf.* (San Diego, CA, June 6-8, 1984), pp. 1836-1842.

[12] R. L. Hollis, "A fine positioning device for enhancing robot precision," in *Proc. Robots 9* (Detroit, MI, June 2-6, 1985), pp. 6.28-6.36.

[13] H. T. Russell, R. L. Hollis, and M. A. Lavin, "Precise manipulation with endpoint sensing," *IBM J. Res. Develop.*, vol. 29, no. 4, pp. 363-376, 1985.

[14] R. L. Hollis *et al.*, "Robotic circuit board testing using fine positioners with fiber optic sensing," in *Proc. Int. Symp. Industrial Robots* (Sept. 11-13, 1985), pp. 315-322.

[15] ——, "A six degree of freedom magnetically levitated variable com-

pliance fine motion wrist," in *Proc. IEEE Int. Conf. Robotics Automat.* (Philadelphia, PA, April 25-29, 1988), pp. 261-269.
[16] J. H. Bruning, "The piezoelectric worm-A submicron linear positioning device," in *Proc. 4th Ann. Symp. Incremental Motion Control Systems and Devices* (Univ. of Illinois-Urbana Champaign, April 1-3, 1975), pp. x-1-x-11.
[17] F. E. Scire and E. C. Teague, "Piezodriven 50 micro stage with subnometer," *Rev. Sci. Instrum.*, vol. 49, no. 12, Dec. 1978.
[18] Y. Umetani, "Principle of a piezoelectric micro manipulator," in *Proc. 8th Int. Symp. Industrial Robots* (Stuttgart, May 30-June 1, 1978), pp. 406-413.
[19] Y. Umetani and H. Suzuki, "Piezoelectric micro-manipulator in multi-degrees of freedom with tactile sensibility," in *Proc 10th Int. Symp. Industrial Robots* (Milan, Mar. 5-7, 1980), pp. 571-579.
[20] R. D. Young, "Moving stage improves accuracy of microcircuit measuring technique," *Res. Develop.*, pp. 114-116, Apr. 1984.
[21] L. H. McCarty, "Piezoelectric actuators generate many motion patterns," *Design News*, pp. 136-138, June 8, 1987.
[22] Z. X. Wang, M. K. Jouaneh, and D. Dornfeld, "Design and characterization of a linear motion piezoelectric microactuator," in *Proc. IEEE Int. Conf. Robotics Automat.* (Scottsdale, AZ, May 14-19, 1989), pp. 1710-1715.
[23] K-M. Lee and S. Arjunan, "Force/torque sensing and micro-motion manipulation of a spherical stepping wrist motor," in *Proc. Amer. Control Conf.* (Atlanta, GA), June 1988.
[24] —, "A three degree of freedom micro-motion in-parallel actuated manipulator," in *Proceedings of the IEEE International Conference on Robotics and Automation* (Scottsdale, Arizona, May 14-19, 1989). pp. 1698-1703, 1989.
[25] I. W. Hunter, S. Lafontaine, P. M. F. Nielsen, P. J. Hunter, and J. M. Hollerbach, "A tele-microrobot for manipulation and dynamic mechanical testing of single living cells," in *Proc. IEEE Workshop Micro Electro Mechanical Systems* (Salt Lake City, UT, Feb. 20-22, 1989), pp. 102-106.
[26] —, "Manipulation and dynamic mechanical testing of microscopic objects using a telemicrorobot system," in *Proceedings of the IEEE Int. Conf. Robotics Automat.* (Scottsdale, AZ, May 14-19, 1989), pp. 1536-1546.
[27] H. S. Tzou, "Development of a light-weight robot end-effector using polymeric piezoelectric bimorph," in *Proc. IEEE Int. Conf. Robotics Automat.* (Scottsdale, AZ, May 14-19, 1989), pp. 1704-1709.
[28] H. S. Tzou, G. C. Wan, and C. I. Tseng, "Dynamics and distributed vibration controls of flexible manipulators: Integrated distributed sensing and active piezoelectric actuator," in *Proc. IEEE Int. Conf. Robotics Automat.* (Scottsdale, AZ, May 14-19, 1989), pp. 1716-1725.
[29] W. Trimmer and R. Jebens, "Actuators for micro robots," in *Proc. IEEE Int. Conf. Robotics Automat.* (Scottsdale, AZ, May 14-19, 1989), pp. 1547-1552.
[30] K-M. Lee and D. Shah, "Kinematic analysis of a three degree of freedom in-parallel actuated manipulator," in *Proc. IEEE Int. Conf. Robotics Automat.* (Raleigh, NC, Mar. 31-Apr. 3, 1987); also in *IEEE J. Robotics Automat.*, vol. 4, no. 2, pp. 354-360, June 1988.
[31] —, "Dynamic analysis of a three degree of freedom in-parallel actuated manipulator," *IEEE J. Robotics Automat.*, vol. 4, no. 2, pp. 361-367, June 1988.
[32] K-M. Lee and R. Johnson, "Static characteristics of an in-parallel actuated manipulator for changing and bracing applications," in *Proc. IEEE Int. Conf. Robotics Automat.* (Scottsdale, AZ, May 14-19, 1989), pp. 1408-1415.
[33] Tokin manufacturer's booklet on multilayer piezoelectric actuators.
[34] M. D. Bryant and R. B. Reeves, "Precision positioning problems using piezoelectric actuators with force transmission through mechanical contact," *Precision Eng.*, vol. 6, no. 3, pp. 129-134, July 1984.
[35] J. Winger and K-M. Lee, "Experimental investigation of a tactile sensor based on bending losses in fiber optics," in *Proc. IEEE Int. Conf. Robotics Automat.* (Philadelphia, PA, Apr. 26-29, 1987).

Kok-Meng Lee (M'89) received the B.S. degree from the State University of New York at Buffalo in 1980 and the S.M. and Ph.D. degrees from the Massachusetts Institute of Technology, Cambridge, in 1982 and 1985, respectively, all in mechanical engineering.

He has been on the Georgia Institute of Technology's Faculty of Mechanical Engineering as an Assistant Professor since 1985; he became an Associate Professor in 1990. His research interests are in the areas of system dynamics, control, robotics, and automation.

Dr. Lee is a recipient of the NSF Presidential Young Investigator Award and the Georgia Tech Sigma Xi Junior Faculty Award.

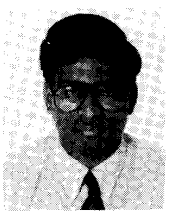

Shankar Arjunan received the B.E. degree from Anna University, Madras, India, in 1984 and the M.S. degree from the Georgia Institute of Technology, Atlanta, in 1988, both in mechanical engineering.

He is currently with the Cummins Engine Company in Columbus, IN, where the is a Controls Engineer in he fuel system controls group for heavy-duty diesel engines.